Study of anion order/disorder in RTaN2O (R = La, Ce, Pr) perovskite nitride oxides

ARTICLE *in* CRYSTAL GROWTH & DESIGN · DECEMBER 2013

Impact Factor: 4.89 · DOI: 10.1021/cg401230a

3 AUTHORS:

Spencer Porter
University of Wollongong
14 PUBLICATIONS **74** CITATIONS
SEE PROFILE

Zhenguo Huang
University of Wollongong
50 PUBLICATIONS **489** CITATIONS
SEE PROFILE

Patrick M. Woodward
The Ohio State University
216 PUBLICATIONS **5,278** CITATIONS
SEE PROFILE

CRYSTAL GROWTH & DESIGN

Article

pubs.acs.org/crystal

Study of Anion Order/Disorder in $RTaN_2O$ (R = La, Ce, Pr) Perovskite Nitride Oxides

Published as part of the Crystal Growth & Design virtual special issue on Anion-Controlled New Inorganic Materials

Spencer H. Porter,[†] Zhenguo Huang,[†] and Patrick M. Woodward*

The Ohio State University, Department of Chemistry & Biochemistry, 100 W. 18th Avenue, Columbus, Ohio 43210

Supporting Information

ABSTRACT: Symmetries and model structures are given for ABN_2O (and $ABNO_2$) perovskites that possess long-range ordering of anions in combination with $a^0a^0c^-$, $a^-b^0a^-$, and $a^-b^+a^-$ octahedral tilting. The stabilities of competing structures have been evaluated using density functional theory (DFT) calculations, which show that *cis*-ordered models are more stable than competing *trans*-ordered polymorphs. To test the validity of these predictions, the perovskite nitride oxides $LaTaN_2O$, $CeTaN_2O$, and $PrTaN_2O$ have been synthesized and characterized using neutron powder diffraction. $CeTaN_2O$ and $PrTaN_2O$ crystallize with orthorhombic *Pnma* symmetry (Ce: a = 5.69666(8), b = 8.03272(9), and c = 5.70893(7) Å; Pr: a = 5.6868(1), b = 8.0153(1), and c = 5.68057(8) Å) as a result of $a^-b^+a^-$ tilting of the octahedra. The structure of $LaTaN_2O$ is re-examined and found to possess orthorhombic *Imma* symmetry (a = 5.7093(1), b = 8.0591(2), and c = 5.7386(2) Å) as a result of $a^-b^0a^-$ tilting. No evidence for long-range anion order is found in any of the three compounds. Optical band gaps for these compounds are measured to be 2.0 eV ($LaTaN_2O$), 1.9 eV ($CeTaN_2O$), and 2.0 eV ($PrTaN_2O$). These values are 0.6−0.7 eV smaller than $CaTaNO_2$ where the Ta-centered octahedra tilt by a similar amount. As the nitrogen content increases, there is an increase in the overlap of the anion 2p orbitals, which increases the energy of the valence band maximum and narrows the band gap.

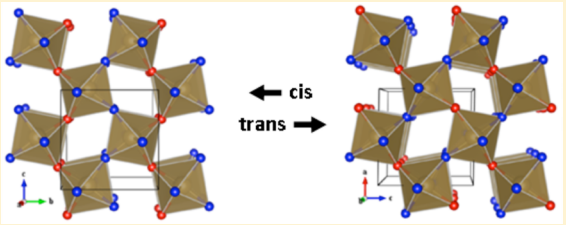

1. INTRODUCTION

Mixed anion systems, and specifically nitride oxides (also widely known as oxynitrides), possess a variety of attractive properties such as superconductivity,[1] high dielectric permittivity,[2,3] photocatalytic activity,[4] and photoluminescence.[5] An evolving question in the literature is whether the anions order in nitride oxides with the perovskite structure, if so what type of ordering exists, and to what extent does the ratio of nitride to oxide ions influence the tendency to order. Literature reports of anion distributions in the nitride oxide perovskites span the spectrum from fully ordered[6] to partially ordered[7−9] to completely disordered.[10,11] Anion ordering has pronounced effects on properties, particularly the dielectric and optical properties, and thus warrants careful studies. For example, density functional theory (DFT) calculations show that three-dimensional (3D) coiled chain motifs of *cis*-$[TaN_{2/2}O_{4/2}]^{2-}$ octahedra can lead to relaxor dielectric behavior.[12]

Initial neutron diffraction studies on the archetypal nitride oxide perovskite, $BaTaNO_2$, reported a cubic structure with $Pm\bar{3}m$ symmetry, and a random O/N distribution.[13] Subsequent studies of the local structure of $BaTaNO_2$ paint a more nuanced picture. Computational studies on large supercells that assume a random distribution of oxide and nitride ions find local distortions of the Ta−N and Ta−O bonds take place that lower the symmetry.[14] This picture is supported by bond distances extracted from extended X-ray absorption fine structure (EXAFS) measurements.[15] A neutron PDF study finds that although long-range anion order is not present in $BaTaNO_2$, on a local scale the $[TaN_{2/2}O_{4/2}]^{2-}$ octahedra predominantly adopt a *cis*-configuration.[16] The preference for a *cis*-configuration in $BaTaNO_2$ is supported by DFT calculations.[18] The observation of sheets of diffuse scattering in electron diffraction experiments reveals one-dimensional correlated displacements of Ta ions.[17]

Turning to other nitride oxide perovskites the picture becomes somewhat less clear. $SrTaNO_2$ and $LaTaN_2O$ have been reported to display *trans*-ordering of the anions,[12] which raises the question of how the larger A-site cation and the O:N ratio impact anion ordering. Subsequent DFT calculations for the $ATaNO_2$ (A = Ba, Sr, Ca) class indicate that *cis*-ordering should be preferred for all three compounds.[18] On the basis of neutron diffraction experiments on $SrTaNO_2$, Fuertes, Attfield, and co-workers have proposed a model where 100% of the $[TaN_{2/2}O_{4/2}]^{2-}$ octahedra adopt a *cis*-configuration, but the −N−Ta−N−Ta−N− linkages form zigzag chains that do not possess long-range translational symmetry.[7] This unusual anion

Received: August 12, 2013
Revised: October 18, 2013
Published: October 31, 2013

arrangement, which is dubbed "open order", shows some parallels to Pauling's ice-rules.[19,20]

To date, most studies of anion ordering in nitride oxide perovskites have concentrated on compounds with $ABNO_2$ (A = Ba, Sr, Ca) stoichiometry. In this study we focus on compounds with $RTaN_2O$ stoichiometry. Syntheses of $RTaN_2O$ perovskites were reported by Marchand and co-workers for R = La, Nd, Sm, Eu, Gd, Dy.[21] In this study, two previously unreported nitride oxides from this family, $CeTaN_2O$ and $PrTaN_2O$, have been synthesized, and their structures were characterized using neutron powder diffraction. In addition, the structure of $LaTaN_2O$ is re-examined.

2. EXPERIMENTAL SECTION

Samples were prepared by a solid state ammonolysis route. Stoichiometric amounts of Ta_2O_5 (99.993%, Alfa Aesar) and the appropriate oxide or hydroxide of the rare earth cation ($La(OH)_3$: 99.99%, GFS Chemicals; Pr_6O_{11}: 99.999%, Cerac; CeO_2: 99.90%, Acros) were ground using a mortar and pestle for 30 min. A NaCl/KCl flux (1:1 by mass) was mixed with the reactants during grinding, with the total mass of the flux being equal to that of the reactants. The NaCl/KCl flux is utilized to increase the mobility of cations by partial solvation.[11] Alumina boats holding the reactants were placed in a tube furnace, and gaseous ammonia was flowed over the sample during annealing. The furnace was ramped at 10 °C/min to 950 °C, held for 20 h, and then cooled at 10−20 °C/min to room temperature. This annealing cycle was repeated four times with grinding between each heating cycle. As a final step, the samples were sequentially triple rinsed with water and acetone to remove any residual flux. $CaTaNO_2$ samples were prepared in a similar manner from a stoichiometric mixture of Ta_2O_5 and $CaCO_3$ (99.99%, Baker). $CaTaNO_2$ is yellow, $LaTaN_2O$ is deep red, $PrTaN_2O$ is maroon, and $CeTaN_2O$ is maroon gray.

The purity of each compound was assessed through Rietveld refinements on powder X-ray diffraction data. Detailed analysis can be found in Supporting Information. To obtain time-of-flight (TOF) neutron powder diffraction data, samples were loaded in vanadium sample cans and data sets were collected at room temperature on the POWGEN BL-11, a neutron powder diffractometer at the Spallation Neutron Source located at Oak Ridge National Laboratory. D-spacings from 0.26 to 6 Å were evaluated using bank 2 and 5 (7000 s, 60 Hz). Rietveld refinements were performed using GSAS as implemented in the EXPGUI macro.[22] Agreement factors presented are from combined refinements of both banks.

DFT calculations were carried out using CASTEP, which employs conjugate gradient minimization, pseudopotentials, and a plane wave basis set. A Kerker scheme norm-conserving, nonlocal pseudopotential (energy cutoff = 400 eV) was employed. An energy charge per atom convergence criterion of 2×10^{-5} eV, a RMS residual force on movable atoms of 0.05 eV/Å, and a root mean square (RMS) displacement of 0.001 Å were selected. Electron exchange interactions and correlation were modeled via the Perdew−Wang '91 GGA functional.[23] Each structure was geometry optimized by the BFGS scheme for subsequent analysis.

UV−visible diffuse reflectance data were collected using an Ocean Optics USB4000-UV−vis spectrometer equipped with a standard reflectance probe and a DH-2000-BAL deuterium/tungsten halogen light source. Data were generated using SpectroSuite software and then transformed by the Kuebelka−Munk method for subsequent interpretation.

3. RESULTS AND DISCUSSION

3.1. Symmetry Analysis for Anion Ordered Perovskites. The symmetry of a mixed anion perovskite depends upon the combination of octahedral tilting and anion ordering that the compound adopts. A symmetry analysis (Figure 1) for the $RTaN_2O$ stoichiometry shows the space group symmetry

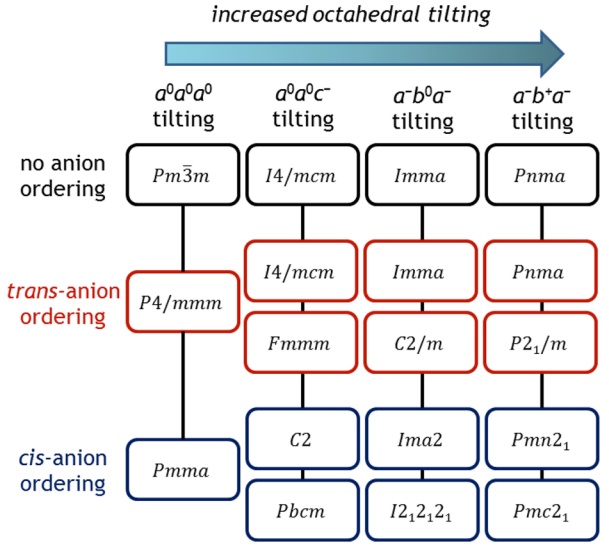

Figure 1. Space groups that result from *cis*- and *trans*-anion ordering and octahedral tilting in mixed anion perovskites.

resulting from the four most common types of octahedral tilting ($a^0a^0a^0$, $a^0a^0c^-$, $a^-b^0a^-$, and $a^-b^+a^-$) in combination with either *cis*- or *trans*-ordering of the oxide ions. Note that the symmetry analysis is identical for the $ATaNO_2$ stoichiometry and *cis*- or *trans*-ordering of the nitride ions.

In the absence of anion ordering, the symmetry is completely dictated by the octahedral tilting. The symmetry consequences of octahedral tilting in perovskites are well established in the literature.[24,25] In the absence of octahedral tilting, *trans*-ordering leads to tetragonal *P*4/*mmm* symmetry, while *cis*-ordering leads to orthorhombic *Pmma* symmetry. For the *trans*-configuration the symmetry could be lowered further to *P*4*mm* by out-of-center displacements of the octahedral cation toward one of the nitride vertices of the octahedron,[16,26] but evidence for that type of distortion in nitride oxide perovskites has not been observed. Consequently, it was not included in our analysis.

When anion ordering and octahedral tilting are both present the symmetry depends on the direction of the two with respect to each other. For example, when there is $a^-b^+a^-$ tilting and *trans*-ordering in an $RTaN_2O$ perovskite, the symmetry is *Pnma* if the −O−Ta−O−Ta− chains run parallel to the axis about which the in-phase rotations occur (i.e., the *b*-axis), but $P2_1/m$ when the −O−Ta−O−Ta− chains run perpendicular to that axis. The four possible combinations of anion ordering and $a^-b^0a^-$ and $a^-b^+a^-$ tilting are illustrated in Figures 2 and 3. Note that for both patterns of tilting there is also a combination that lowers the symmetry to triclinic *P*1, but this possibility was not considered in detail due to parsimony considerations[27] and the lack of any experimental evidence suggesting triclinic symmetry.

3.2. NPD Structure Refinements. To identify octahedral tilting in these compounds, the method outlined by Barnes et al. was used.[28] The patterns were indexed on a doubled cubic perovskite unit cell. Superstructure reflections for $LaTaN_2O$ were all of the <ooo> type. These reflections are indicative of out-of-phase tilting of the octahedra, and thus an *Imma* starting model was selected. Other symmetries that are associated exclusively with out-of-phase tilts (*F*1, *I*2/*a*, $R\bar{3}c$, *I*2/*m*, and *I*4/*mcm*) were considered but were discarded because refinements using these space groups gave inferior fits to the diffraction

dx.doi.org/10.1021/cg401230a | Cryst. Growth Des. 2014, 14, 117−125

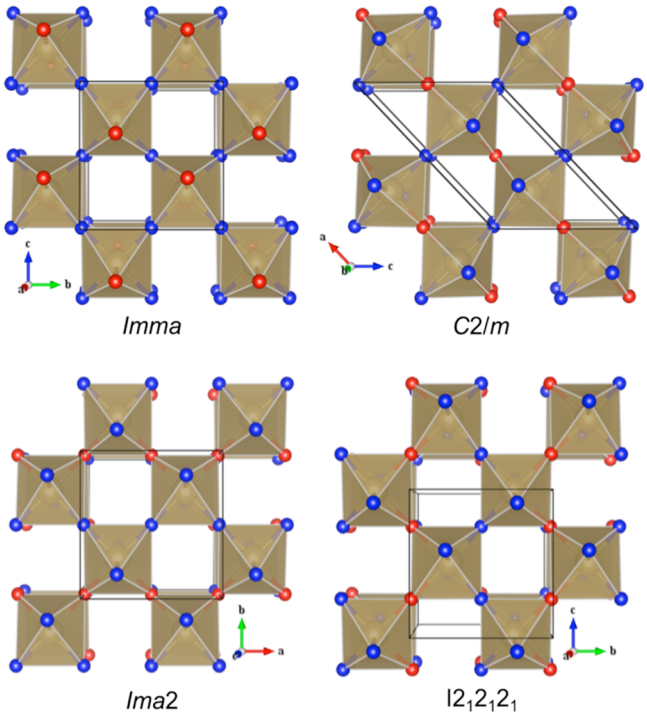

Figure 2. Fully anion ordered trans (top) and cis (bottom) models in $a^-b^0a^-$ tilted perovskite $RTaN_2O$ systems. Blue spheres represent nitrogen and red spheres oxygen. A-site cations are not shown for clarity. Models are viewed down the axis about which no tilting occurs.

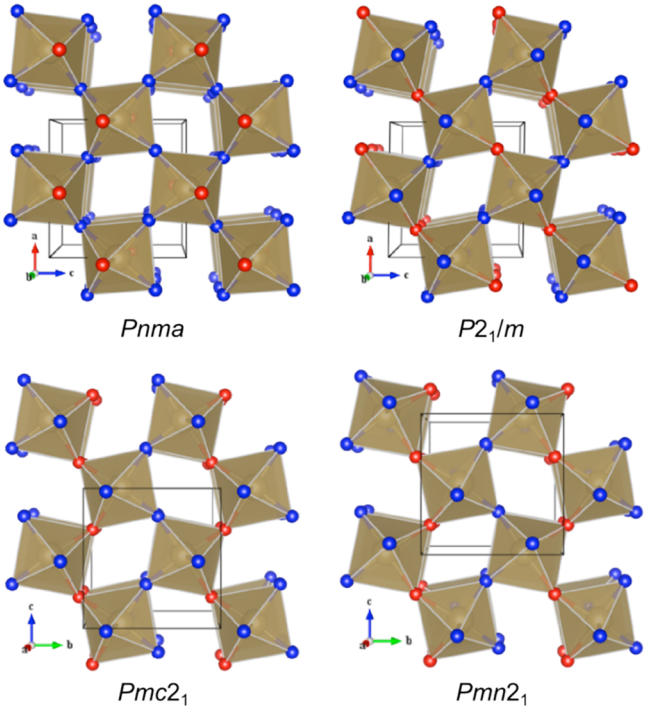

Figure 3. Fully anion ordered trans (top) and cis (bottom) models in $a^-b^+a^-$ tilted perovskite $RTaN_2O$ systems. A-site cations are not shown for clarity. Models are viewed down the axis about which in-phase tilting occurs.

data. For $CeTaN_2O$ and $PrTaN_2O$, the diffraction patterns also contain superstructure reflections that could be classified as <eeo> and <ooe> (see Figure 4). The presence of <ooe> reflections indicates in-phase tilting, while <eeo> reflections are

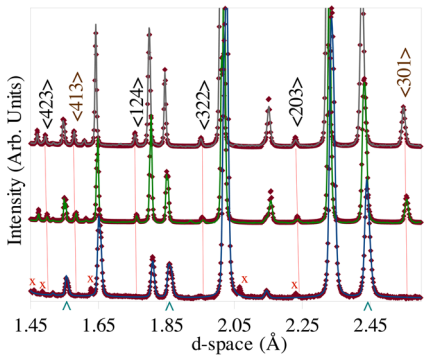

Figure 4. Neutron powder diffraction patterns for $RTaN_2O$ (R = La, Ce, Pr). Purple diamonds are observed data, while the blue (La), green (Ce), and gray (Pr) lines are the calculated diffraction patterns. Peaks arising from an unidentified secondary phase in the $LaTaN_2O$ pattern are marked with an *x*. The reflections with ooo indices are marked with a turquoise caret at the bottom. The Miller indices (as indexed on a double cubic cell) for those reflections with ooe (brown) and eeo (black) are given at the top. Red vertical lines are a guide to the eye to follow the positions of those reflections as the unit cell changes.

associated with displacements of the R^{3+} ions that only occur when both in-phase and out-of-phase tilts exist. The presence of all three classes of superstructure reflections is typically associated with $a^-b^+a^-$ tilting and *Pnma* space group symmetry. Once again, other tilt systems that combine in-phase and out-of-phase tilts (*Pmmn* and $P2_1/m$) were considered but rejected because they did not produce a good fit to the diffraction data.

With the octahedral tilt patterns confirmed as $a^-b^0a^-$ for $LaTaN_2O$, and $a^-b^+a^-$ for $CeTaN_2O$ and $PrTaN_2O$, starting models corresponding to various anion ordering patterns given in Figures 1−3 were used in refinements of the neutron powder diffraction data. For each compound, refinements were carried out based on five models of anion ordering: (1) a random distribution where the occupancies of all anions sites are fixed at 2/3 N and 1/3 O, (2) long-range *trans*-ordering of oxygen, (3) long-range *cis*-ordering of oxygen, (4) a structure where the oxide ions are confined to layers, but with open order and a local *cis*-configuration within those layers (as found in $SrTaNO_2$ by Yang et al.),[7] and (5) free refinement of the occupancies with a constraint that the overall stoichiometry must remain $RTaN_2O$. For models (1), (4), and (5), the space group symmetry is *Imma* for R = La and *Pnma* for R = Ce, Pr. For the fully ordered models, (2) and (3), each type of symmetry shown in Figure 1 was tested.

The goodness of fit parameters obtained from the refinements are summarized in Table 1 for $LaTaN_2O$ and Table 2 for $RTaN_2O$ (R = Ce, Pr). For all three compounds, the *trans*-ordered (2) and *cis*-ordered (3) models give inferior fits to the data, while a random distribution of anions gives a very good fit. This observation allows us to rule out long-range anion ordering in all three compounds. When the occupancies are allowed to refine, model (5), the occupancies refine to values not too far from the random model, and there is effectively no change in the goodness of fit parameter. There is no evidence for the confinement of the O ions into layers, as reported for $SrTaNO_2$,[7] but because model (4) gives a similar fit to models (1) and (5) it cannot be ruled out. In particular, the occupancies obtained when using model (5) to fit the $PrTaN_2O$ pattern are intermediate between a random distribution, model (1), and the layered open order of model (4). As documented in ref 7, the ability to distinguish different

dx.doi.org/10.1021/cg401230a | *Cryst. Growth Des.* 2014, 14, 117−125

Table 1. Fits to $LaTaN_2O$ Neutron Powder Diffraction Data for Various Models of Anion Ordering

	(1) random	(2a) *trans*-ordered	(2b) *trans*-ordered	(3a) *cis*-ordered	(3b) *cis*-ordered	(4) 2D *cis*-ordered	(5) fixed stoichiometry
space group	*Imma*	*Imma*	*C*2/*m*	*Ima*2	$I2_12_12_1$	*Imma*	*Imma*
anion site occupancies	[4e] O = 0.33 N = 0.67	[8g] N = 1	[4g], [4i] N = 1	[4a], [4b] N = 1	[4a], [4c] N = 1	[8g] O = 0.25 N = 0.75	[8g] O = 0.328(7) N = 0.672(7)
	[8g] O = 0.33 N = 0.67	[4e] O = 1	[4h] O = 1	[4a] O = 1	[4a] O = 1	[4e] O = 0.5 N = 0.5	[4e] O = 0.34(1) N = 0.66(1)
R_{wp} (%)	2.38	3.15	2.54	2.73	2.66	2.44	2.38

Table 2. Fits to $CeTaN_2O$ and $PrTaN_2O$ Neutron Powder Diffraction Data Sets for Various Models of Anion Ordering

	(1) random	(2a) *trans*-ordered	(2b) *trans*-ordered	(3a) *cis*-ordered	(3b) *cis*-ordered	(4) 2D *cis*-ordered	(5) fixed stoichiometry
space group	*Pnma*	*Pnma*	$P2_1/m$	$Pmn2_1$	$Pmc2_1$	*Pnma*	*Pnma*
anion site occupancies	[4e] O = 0.33 N = 0.67	[8g] N = 1	[4f], [2e], [2e] N = 1	[2a], [2a], [4b] N = 1	[2a], [2b], [4c] N = 1	[8g] O = 0.25 N = 0.75	[8g][a] O = 0.314(4) N = 0.686(4)
	[8g] O = 0.33 N = 0.67	[4e] O = 1	[4f] O = 1	[4b] O = 1	[4c] O = 1	[4e] O = 0.5 N = 0.5	[4e] O = 0.372(8) N = 0.628(8)
R_{wp} (%) (R = Ce)	2.50	4.10	2.66	3.34	3.58	2.56	2.50
R_{wp} (%) (R = Pr)	2.32	3.27	2.48	2.76	2.73	2.33	2.31

[a]Occupancies are for R = Ce. The occupancies for R = Pr: O = 0.288(6), N = 0.712(6) for the [8g] site, and O = 0.42(1), N = 0.58(1) for the [4e] site.

models of ordering from the neutron data is quite sensitive to the splitting of the peaks, and here the orthorhombic distortion (and hence peak splitting) is largest in $PrTaN_2O$. This may be an indication that some degree of layering of the oxide ions is present here.

A summary of the lattice parameters is given in Table 3. The final Rietveld refinement fits are presented in Figure 5. The peak misfit at higher d-spacing (>2.0 Å) is consistent for all patterns and could not be remedied. This artifact is presumably due to a subtle and systematic error in the calibration of the detector modules. Atomic coordinates for $LaTaN_2O$, $CeTaN_2O$, and $PrTaN_2O$ are listed in Tables 4, 5, and 6, respectively. Isotropic displacement parameters were used for the cations, while anisotropic displacement parameters were used for anions. All parameters for anions that share a common site were constrained to be equal.

Table 3. Lattice Parameters and Refinement Results for $RTaN_2O$ System (R = La, Ce, Pr)

compound	$LaTaN_2O$	$CeTaN_2O$	$PrTaN_2O$
space group	*Imma*	*Pnma*	*Pnma*
Z	4	4	4
a (Å)	5.7093(1)	5.69666(8)	5.6868(1)
b (Å)	8.0591(2)	8.03272(9)	8.0153(1)
c (Å)	5.7386(2)	5.70893(7)	5.68057(8)
V (Å^3)	264.04(2)	261.239(8)	258.929(8)
R_p (%)	3.30	3.35	3.37
R_{wp} (%)	2.38	2.50	2.32
χ^2	5.874	7.134	5.685

$LaTaN_2O$ has previously been reported to possess *C*2/*m* symmetry.[6] Our symmetry analysis shows this assignment would be consistent with $[TaN_{4/2}O_{2/2}]^{3-}$ octahedra that have a *trans*-configuration and $a^-b^0a^-$ tilting. Our results confirm the $a^-b^0a^-$ pattern of octahedral tilting but do not support the assignment of long-range *trans*-ordering. To check the validity of our assignment, we carried out refinements of $LaTaN_2O$ using *C*2/*m* symmetry. It is true that this model (R_{wp} = 2.54%) gives a better fit than a fully ordered *Imma* model (model (2a) also with *trans*-ordering, R_{wp} = 3.15%), but the fit is inferior compared to *Imma* with a random distribution of anions (R_{wp} = 2.38%). Interestingly, refinement of only bank 2 data, similar to what Jansen and co-workers presented,[6] gives a slightly better fit for *C*2/*m*. However, when bank 5 data are included in the combined refinements, the *C*2/*m* model poorly fits the peak at 4.05 Å, and the overall fit for a random anion distribution in *Imma* becomes lower (see Supporting Information for full details). It should also be noted that when the occupancies of the anions were allowed to refine in *C*2/*m*, they moved to values indicative of a random distribution. In the absence of *trans*-ordering, the justification for *C*2/*m* symmetry is not clear. Finally, we note that the systematic absences are such that there are superstructure peaks allowed in *C*2/*m* that are forbidden in *Imma*. No appreciable intensity was observed at those peak positions in the neutron diffraction pattern. Therefore, we conclude that the symmetry of $LaTaN_2O$ is *Imma* and not *C*2/*m*. There are a few weak reflections seen in the NPD pattern of $LaTaN_2O$ that could not be indexed or fit to any model of anion ordering. These small reflections appear to arise from the presence of a trace amount of a secondary phase.

As the nitrogen content increases, the average Ta−X bond distances in comparable tantalum compounds increase (Table 7) from in 1.99 Å in $KTaO_3$,[29] to approximately 2.02 Å in $CaTaNO_2$[11] and $SrTaNO_2$,[11] to 2.04−2.06 Å in $RTaN_2O$, and finally to 2.09 Å in Ta_3N_5.[30] This follows the trend that would be expected based on the larger ionic radii of the nitride ion (1.46 Å, 4 coordinate) vs the oxide ion (1.38 Å, 4 coordinate).[31] The Ta−X bond distances in $BaTaNO_2$ are an outlier. We postulate that $BaTaNO_2$ does not follow the trend for the same reason that the average bond distance in $BaTiO_3$ is larger than in $SrTiO_3$ and $CaTiO_3$. Namely, that Ba is too big for the network of corner connected octahedra and out-of-center displacements of the Ti ions occur, leading to an expansion in the average Ti−O distance. While there is no evidence for cooperative out-of-center displacements in $BaTaNO_2$, there is substantial evidence for local out-of-center displacements.[15,16]

The Ta−X−Ta angle (Table 7) decreases as the size of the A-site cation decreases Ba > Sr > > La > Ce > Pr ∼ Ca, in line

dx.doi.org/10.1021/cg401230a | *Cryst. Growth Des.* 2014, 14, 117−125

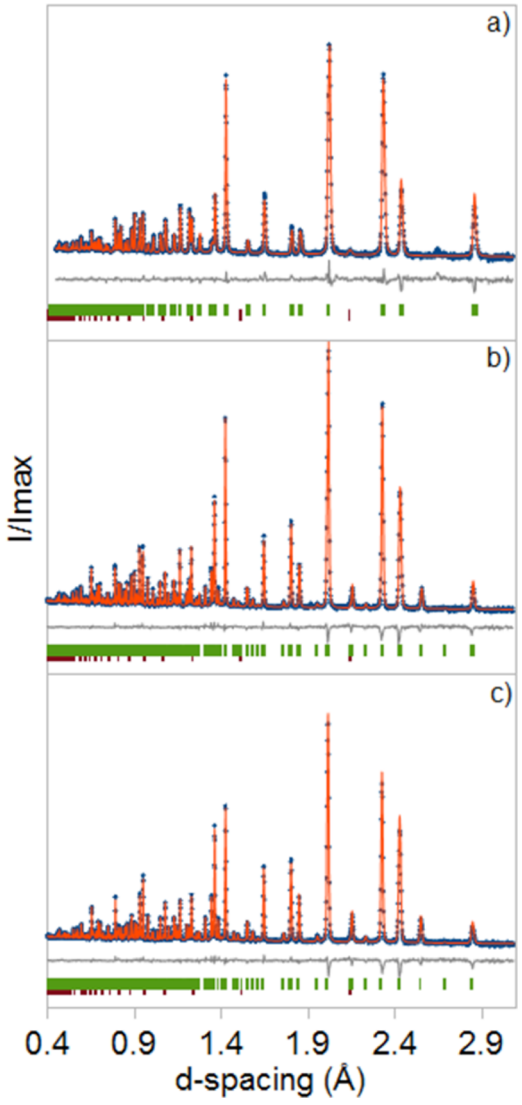

Figure 5. Rietveld refinements of bank 2 NPD data for (a) $LaTaN_2O$, (b) $CeTaN_2O$, and (c) $PrTaN_2O$. Blue dots represent experimental data, a red line the calculated pattern, and a gray line the difference curve. Green hash marks show the reflection positions for the perovskite phase, and cyan hash marks the reflection positions for the vanadium sample holder.

with the decrease in the tolerance factor. From the anion positions, it is possible to extract the magnitude of the out-of-phase and in-phase tilts using the equations first formulated by Hyde and O'Keeffe et al.[32] and verified by TUBERS, a subprogram of SPUDS.[33] The octahedra in $LaTaN_2O$ have out-of-phase tilts, φ, just over 10°, and have no in-phase tilt, ψ, as required by the *Imma* symmetry. The in-phase tilts for both $CeTaN_2O$ and $PrTaN_2O$ are nonzero but small, as one might expect given the fact that these compounds have tolerance factors only slightly smaller than $LaTaN_2O$. Finally in $CaTaNO_2$ both the in-phase and out-of-phase tilts are larger still. The observation that the out-of-phase tilts are much larger than the in-phase tilts, is also observed in oxide perovskites with $a^-b^+a^-$ tilting. For example, $SrZrO_3$, which has a similar tolerance factor (τ = 0.95) has tilts of φ = 11.93° and ψ = 0.59°.[34]

3.3. Electronic Structure Calculations. While it is known from previous computational work that *cis* models yield lower overall lattice enthalpies for perovskites with $ATaNO_2$ stoichiometry,[16,18,35] whether the preference for the *cis*-configuration extends to perovskites with a 1:2 ratio of oxygen to nitrogen (e.g., $LaTaN_2O$) has not been established. To investigate if changing from $ATaNO_2$ to $ATaN_2O$ has any effect on the *cis*- vs *trans*-competition, we calculated the enthalpies of geometry optimized $CaTaNO_2$ and $LaTaN_2O$ in each of the anion ordered model structures shown in Figures 2 and 3. For each composition, we constrained the octahedral tilting to the pattern that has been verified experimentally: $a^-b^+a^-$ tilting for $CaTaNO_2$ and $a^-b^0a^-$ for $LaTaN_2O$. Full crystallographic details for each geometry optimized calculated structure can be found in the Supporting Information.

The enthalpies (normalized on a per formula unit basis) for $CaTaO_2N$ are shown in Figure 6 and those for $LaTaN_2O$ are in Figure 7. The lattice enthalpies of the *cis*-configurations are 150−250 meV more stable than those of either *trans*-configuration, revealing a similar preference for the *cis*-configuration in both compounds. The enthalpic preference for a *cis*-configuration, coupled with the earlier report that the molar configurational entropies of $ABNO_2$ and ABN_2O are identical,[19] leads to the conclusion that both stoichiometries should show a strong preference for a local *cis*-configuration. The fact that there are multiple *cis*-ordered configurations with similar enthalpies helps to explain why the tendency for a local *cis*-configuration does not lead to long-range anion ordering.

The preference for a *cis*-configuration is consistent with the behavior of other compounds containing d^0 cations that are octahedrally coordinated by ligands with different electronegativities. In ordered structures, the ligands that form more covalent bonds with the metal (M−F < M−O < M−N) are nearly always located adjacent to each other. This leads to a *cis*-

Table 4. Coordinates and Displacement Parameters for $LaTaN_2O$ with *Imma* Symmetry

atomic position(s)						
ion	site	x	y	z	occ	U_{iso} (Å^2)
Ta^{5+}	4b	0	0	0	1	0.0058(2)
La^{3+}	4c	0	0.25	0.5	1	0.0104(2)
O/N	4c	0	0.25	0.0677(3)	0.33/0.67	0.0146[a]
O/N	8d	0.25	0.9658(1)	0.25	0.33/0.67	0.0201[a]
anisotropic displacement parameters of the anions						
site	U_{11}	U_{22}	U_{33}	U_{12}	U_{13}	U_{23}
4c	0.033(1)	0.0036(6)	0.0070(5)	0	0	0
8d	0.9172(7)	0.0187(5)	0.0246(8)	0	−0.0147(5)	0

[a]Value listed is U_{eqv}.

dx.doi.org/10.1021/cg401230a | *Cryst. Growth Des.* 2014, 14, 117−125

Table 5. Coordinates and Displacement Parameters for $CeTaN_2O$ with Pnma Symmetry

atomic position(s)						
ion	site	x	y	z	occ	U_{iso} (Å^2)
Ta^{5+}	4b	0.5	0	0	1	0.0075(1)
Ce^{3+}	4c	0.0187(3)	0.25	0.9962(4)	1	0.0083(2)
O/N	4c	0.4897(3)	0.25	0.0755(2)	0.33/0.67	0.0117[a]
O/N	8d	0.2760(1)	0.03901(7)	0.7244(1)	0.33/0.67	0.0133[a]
anisotropic displacement parameters of the anions						
site	U_{11}	U_{22}	U_{33}	U_{12}	U_{13}	U_{23}
4c	0.0190(6)	0.0040(3)	0.0120(4)	0	−0.0014(5)	0
8d	0.0115(3)	0.0171(3)	0.0112(3)	−0.0024(3)	−0.0087(2)	0.0014(3)

[a]Value listed is U_{eqv}.

Table 6. Coordinates and Displacement Parameters for $PrTaN_2O$ with *Pnma* Symmetry

atomic position (S)						
ion	site	x	y	z	occ	U_{iso} (Å^2)
Ta^{5+}	4b	0.5	0	0	1	0.0063(1)
Pr^{3+}	4c	0.0249(3)	0.25	0.9972(6)	1	0.0090(3)
O/N	4c	0.4864(3)	0.25	0.0785(2)	0.33/.67	0.0100[a]
O/N	8d	0.2829(2)	0.04003(9)	0.7203(2)	0.33/.67	0.0112[a]
anisotropic displacement parameters of the anions						
site	U_{11}	U_{22}	U_{33}	U_{12}	U_{13}	U_{23}
4c	0.0165(8)	0.0035(4)	0.0100(6)	0	0.0005(5)	0
8d	0.0097(4)	0.0148(3)	0.0090(4)	−0.0021(4)	−0.0074(3)	−0.0003(3)

[a]Value listed is U_{eqv}.

Table 7. NPD Determined Bond Parameters for the $RTaN_2O$ (R = La, Ce, Pr) and $ATaNO_2$ (A = Ca, Sr, Ba)[a]

compound	$BaTaNO_2$	$SrTaNO_2$	$CaTaNO_2$	$LaTaN_2O$	$CeTaN_2O$	$PrTaN_2O$
tolerance factor	1.03	0.97	0.94	0.93	0.93	0.91
d_{M-X} (Å)	2.0564	2 × 2.02042 4 × 2.02276	2 × 2.0189 2 × 2.02126 2 × 2.04024	2 × 2.0526(3) 4 × 2.0435(1)	2 × 2.0551(2) 2 × 2.0532(6) 2 × 2.0491(6)	2 × 2.040(1) 2 × 2.0556(4) 2 × 2.060(1)
M−X−M angle (°)	180	171.718	153.3308	158.0(1)	155.47(9)	154.2(1)
		180	155.1314	164.0(9)	158.83(7)	157.2(1)
φ (°)	0	3.8	14.6	10.099(3)	10.455(8)	11.81(1)
ψ (°)	0	0	0.882	0	0.4509(3)	0.5762(6)

[a]$ATaNO_2$ data are from refs 11, 6, and 13, respectively.

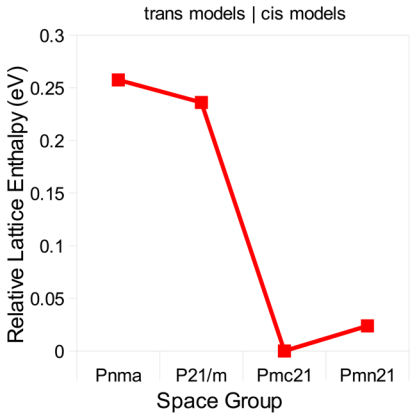

Figure 6. DFT calculated energies for anion ordered $CaTaNO_2$ structures with $a^-b^+a^-$ tilting. The lowest energy structure is set to zero energy. All values are normalized per $CaTaNO_2$ formula unit.

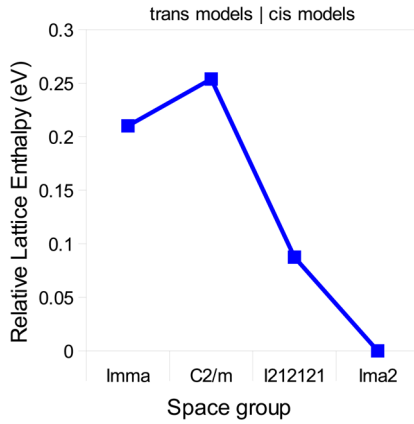

Figure 7. DFT calculated energies for anion ordered $LaTaN_2O$ structures with $a^-b^0a^-$ tilting. The lowest energy structure is set to zero energy. All values are normalized per $LaTaN_2O$ formula unit.

configuration in compounds like $(NH_4)_2MoO_2F_4$,[36] where the d^0 metal ion is coordinated by two oxide and four fluoride ligands, and a *fac*-configuration in compounds like $AgNa(VO_2F_2)_2$,[37] and $Ag_{1.5}Na_{1.5}MoO_3F_3$,[38] where the d^0 metal ion is

dx.doi.org/10.1021/cg401230a | Cryst. Growth Des. 2014, 14, 117−125

coordinated by three oxide and three fluoride ligands. These arrangements, which avoid placing the ligands that form more covalent bonds on opposite sides of the octahedron, seem to be preferred for optimizing the metal dπ−anion pπ interactions to the less electronegative ligand.[18,39] In $RTaN_2O$, four of the six ligands are nitrogen, so it is not possible to avoid placing the ligands that form more covalent bonds on opposite sides of the metal, but the *cis*-configuration produces fewer linear N−Ta−N bonds (one per octahedron) than the *trans*-configuration (two per octahedron).

Even though the calculations underestimate the experimental band gaps, a phenomenon that is seen elsewhere,[40−42] the trends in band gap energies are meaningful. As Tables 8 and 9 show, in all cases the *cis*-ordered structures have larger calculated band gaps than the *trans*-ordered structures. Larger band gaps are typically associated with structures that show a higher degree of stability.[43−45] This finding, and the preference for a *cis*-configuration, agree with the earlier computational studies by Dronskowski et al. on $CaTaNO_2$.[18] We also note that the band gaps for $LaTaN_2O$ are 0.5−0.6 eV smaller than for $CaTaNO_2$, which as we will see in the next section is in good agreement with experiment.

Table 8. DFT Generated Energies, Band Gaps, and Bond Parameters for the $CaTaNO_2$ $a^-b^+a^-$ Systems

space group	*Pnma*	$P2_1/m$	$Pmc2_1$	$Pmn2_1$
relative lattice enthalpy (meV)	+258	+236	0	+24
E_g (eV)	0.596	0.760	1.277	1.495
Ta−N (Å)	2 × 2.093	Ta(1) 2 × 2.089	2.0458	2.0179
		Ta(2) 2 × 2.090	2.0104	2.0349
Ta−O (Å)	2 × 2.127	Ta(1) 2 × 2.118	2.2177	2.0869
	2 × 2.126	Ta(1) 2 × 2.127	2.1489	2.1034
		Ta(2) 2 × 2.116	2.1046	2.1695
		Ta(2) 2 × 2.119	2.0869	2.1868
Ta−N−Ta (°)	156.9	150.4	149.4	146.4
Ta−O−Ta (°)	144.0	144.1	149.8	147.3
		142.3	143.8	141.7
		145.1	133.7	139.5

Table 9. DFT Generated Lattice Energies, Band Gaps, and Bond Parameters for the $LaTaN_2O$ $a^-b^0a^-$ System

space group	*C*2/*m*	*Imma*	$I2_12_12_1$	*Ima*2
relative lattice enthalpy (meV)	+253	+210	+88	0
E_g (eV)	0.445	0.201	0.718	1.076
Ta−N (Å)	2 × 2.1389	4 × 2.1399	2 × 2.1437	2.3517
	2 × 2.1377		2 × 2.0522	2 × 2.048
				2.0122
Ta−O (Å)	2 × 2.1392	2 × 2.1450	2 × 2.2354	2 × 2.2446
Ta−N−Ta (°)	168.4	156.4	158.8	157.0
	148.9		150.8	146.6
Ta−O−Ta (°)	148.3	148.2	154.1	142.5

3.4. Diffuse Reflectance of $CaTaNO_2$ and $RTaN_2O$ where R = La, Ce, Pr. Diffuse reflectance spectra (Figure 8) enable quantitative comparison of the optical band gaps of these four compounds. The band gaps, which were estimated using the Shapiro method,[46] were found to be 2.6, 2.0, 2.0, and 1.9 eV for $CaTaNO_2$, $LaTaN_2O$, $PrTaN_2O$, and $CeTaN_2O$, respectively. As expected, there is a strong correlation between the band gaps and the observed colors—yellow ($CaTaNO_2$),

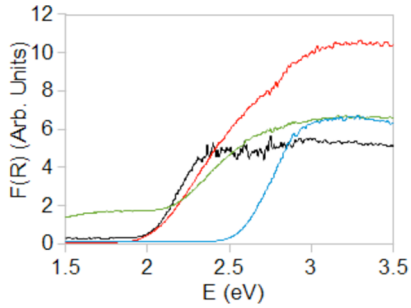

Figure 8. Kuebelka−Monk transformed UV−visible diffuse reflectance patterns for $CaTaNO_2$ (blue), $LaTaN_2O$ (black), $PrTaN_2O$ (red), and $CeTaN_2O$ (green).

red ($LaTaN_2O$), maroon ($PrTaN_2O$), and maroon gray ($CeTaN_2O$). It has been shown elsewhere that in perovskites containing d^0 ions as the magnitude of octahedral tilting increases, the width of the conduction band narrows and the band gap decreases.[47] This effect is largely responsible for the increase in band gap seen in the $ATaNO_2$ (A = Ca, Sr, Ba) perovskites as the size of the A cation decreases from Ba > Sr > Ca.[11,48] The Ta−X−Ta angles in $RTaN_2O$ (R = La, Ce, Pr) are very similar to those in $CaTaNO_2$, but the observed band gap in the latter compound is 0.6 eV larger. The smaller band gap of the $RTaN_2O$ perovskites with respect to $CaTaNO_2$ is primarily due to changes in the position of the valence band maximum. The orbital character at the top of the valence band is largely nonbonding anion 2p. Small overlap between 2p orbitals on neighboring anions gives rise to weak antibonding character and some dispersion in these bands. Because the N 2p orbitals (Dirac−Fock, r_{max} = 0.52 Å) are larger than the O 2p orbitals (r_{max} = 0.44 Å) the 2p−2p overlap increases as the nitrogen content increases, leading to more antibonding character. This causes an increase in the energy of the valence band maximum and a narrowing of the band gap. A recent study of the band edge positions in $ATaNO_2$ (A = Ca, Sr, Ba) and $PrTaN_2O$ provides direct experimental support for this picture.[48]

Although all three $RTaN_2O$ compounds have similar band gaps, the color of $CeTaN_2O$ is darker than the other two. We hypothesize that this effect originates from the presence of Ce 4f states in the band gap. Transitions from these localized 4f levels into the empty conduction band lead to absorption of photons with energies below the band gap (see Figure 8) and are responsible for the darker color. Similar behavior has been seen in the color of oxides like $CeVO_4$.[49] This effect is not observed for Pr, presumably because the 4f orbitals are lower in energy (due to the increase in effective nuclear charge) and no longer lie in the band gap.

4. CONCLUSION

Symmetries and model structures are given for ABN_2O (and $ABNO_2$) perovskites that possess long-range ordering of anions in combination with $a^0a^0c^-$, $a^-b^0a^-$, and $a^-b^+a^-$ octahedral tilting. The crystal structures of $RTaN_2O$ where R = Ce, Pr are reported for the first time, while the structure of $LaTaN_2O$ is revisited. $CeTaN_2O$ and $PrTaN_2O$ have $a^-b^+a^-$ octahedral tilting and exhibit no long-range ordering of anions, a combination that leads to *Pnma* symmetry. There is no evidence for long-range anion ordering in $LaTaN_2O$ either, but the pattern of octahedral tilting is different, $a^-b^0a^-$, which results in *Imma* symmetry. DFT calculations show that ordered structures where the $[TaN_{4/2}O_{2/2}]^{3-}$ octahedra adopt a *cis*-

dx.doi.org/10.1021/cg401230a | *Cryst. Growth Des.* 2014, 14, 117−125

configuration are considerably more stable than those where the octahedra adopt a *trans*-configuration. However, alternate patterns of long-range ordering that retain the local *cis*-configuration have very similar enthalpies. The fact that there are multiple *cis*-ordered configurations with similar enthalpies helps to explain why the strong preference for a local *cis*-configuration does not lead to long-range anion ordering. These conclusions hold for both $ATaNO_2$ and $RTaN_2O$ stoichiometries. The findings here are consistent with recent experimental and computational work on the anion distribution in $SrTaNO_2$.[7,12,19]

Diffuse reflectance data reveal band gaps of 1.9 eV for $CeTaN_2O$, 2.0 eV for $PrTaN_2O$, and 2.0 eV for $LaTaN_2O$. These values are approximately 0.6−0.7 eV smaller than $CaTaNO_2$ which shows a similar degree of octahedral tilting. Overlap of filled anion 2p orbitals becomes more pronounced as the nitrogen content increases, pushing up the energy of the valence band maximum and decreasing the band gap.

■ ASSOCIATED CONTENT

Ⓢ Supporting Information

Atomic and lattice parameters for the DFT calculations. XRD patterns for $RTaN_2O$ (R = La, Ce, Pr). This material is available free of charge via the Internet at http://pubs.acs.org.

■ AUTHOR INFORMATION

Corresponding Author

*E-mail: woodward@chemistry.ohio-state.edu.

Present Address

[†](S.H.P. and Z.H.) Institute for Superconducting and Electronic Materials, University of Wollongong, Wollongong, New South Wales 2522, Australia.

Funding

This work was supported by NSF Grant DMR-0907356.

Notes

The authors declare no competing financial interest.

■ ACKNOWLEDGMENTS

Financial support from the National Science Foundation (Award number DMR-0907356) is acknowledged. The authors would like to thank Ashfia Huq at ORNL for assistance with the neutron data collection & Young-Il Kim at Yeungnam University for helpful discussions.

■ ABBREVIATIONS

NPD, neutron powder diffraction; PDF, pair distribution function; TOF, time-of-flight; SNS, Spallation Neutron Source; ORNL, Oak Ridge National Laboratory; DFT, density functional theory; CASTEP, Cambridge Serial Total Energy Package; RMS, root-mean-square; GGA, generalized gradient approximation; BFGS, Broyden-Fletcher-Goldfarb-Shanno; <ooo>, <odd odd odd>; <eeo>, <even even odd>; <eoo>, <even odd odd>; SPUDS, Structure Prediction Diagnostic Software; CBM, conduction band maximum; VBM, valence band maximum; KPFM, Kelvin probe force microscopy; XPS, X-ray photoelectron spectroscopy; DRCLS, depth-resolved cathodoluminescence spectroscopy

■ REFERENCES

(1) Tobias, G.; Oro-Sole, J.; Beltran-Porter, D.; Fuertes, A. *Inorg. Chem.* **2001**, *40* (27), 6867−6869.
(2) Kim, Y.-I.; Woodward, P. M. *Ceram. Trans.* **2005**, *169*, 179−186.
(3) Marchand, R.; Pors, F.; Laurent, Y.; Regreny, O.; Lostec, J.; Haussonne, J. M. *J. Phys. Colloques* **1986**, *47*, C1-901−C1-905.
(4) Maeda, K.; Domen, K. *J. Phys. Chem. C* **2007**, *111* (22), 7851−7861.
(5) Li, Y. Q.; Delsing, A. C. A.; de With, G.; Hintzen, H. T. *Chem. Mater.* **2005**, *17* (12), 3242−3248.
(6) Gunther, E.; Hagenmayer, R.; Jansen, M. *Z. Anorg. Allg. Chem.* **2000**, *626*, 1519−1525.
(7) Yang, M.; Oro-Sole, J.; Rodgers, J. A.; Jorge, A. B.; Fuertes, A.; Attfield, J. P. *Nat. Chem.* **2011**, *3* (1), 47−52.
(8) Ebbinghaus, S. G.; Weidenkaff, A.; Rachel, A.; Reller, A. *Acta Crystallogr. C* **2004**, *60* (9), i91−i93.
(9) Oró-Solé, J.; Clark, L.; Bonin, W.; Attfield, J. P.; Fuertes, A. *Chem. Commun.* **2013**, *49*, 2430−2.
(10) Clarke, S. J.; Hardstone, K. A.; Michie, C. W.; Rosseinsky, M. J. *Chem. Mater.* **2002**, *14*, 2664−2669.
(11) Kim, Y.-I.; Woodward, P. M.; Baba-Kishi, K. Z.; Tai, C. W. *Chem. Mater.* **2004**, *16* (7), 1267−1276.
(12) Hinuma, Y.; Moriwake, H.; Zhang, Y.-R.; Motohashi, T.; Kikkawa, S.; Tanaka, I. *Chem. Mater.* **2012**, *24* (22), 4343−4349.
(13) Pors, F.; Marchand, R.; Laurent, Y.; Bacher, P.; Roult, G. *Mater. Res. Bull.* **1988**, *23* (10), 1447−1450.
(14) Fang, C. M.; de Wijs, G. A.; Orhan, E.; de With, G.; de Groot, R. A.; Hintzen, H. T.; Marchand, R. *J. Phys. Chem. Solids* **2003**, *64*, 281−286.
(15) Ravel, B.; Kim, Y.-I.; Woodward, P. M.; Fang, C. M. *Phys. Rev. B* **2006**, *73*, 184121.
(16) Page, K.; Stoltzfus, M. W.; Kim, Y. I.; Proffen, T.; Woodward, P. M.; Cheetham, A. K.; Seshadri, R. *Chem. Mater.* **2007**, *19* (16), 4037−4042.
(17) Withers, R. L.; Liu, Y.; Woodward, P. M.; Kim, Y.-I. *Appl. Phys. Lett.* **2008**, *92*, 102907.
(18) Wolff, H.; Dronskowski, R. *J. Comput. Chem.* **2008**, *29* (13), 2260−2267.
(19) Camp, P. J.; Fuertes, A.; Attfield, J. P. *J. Am. Chem. Soc.* **2012**, *134* (15), 6762−6766.
(20) Pauling, L. *J. Am. Chem. Soc.* **1935**, *57*, 2680−2684.
(21) Marchand, R.; Pors, F.; Laurent, Y. *Ann. Chim. Sci. Mater.* **1991**, *16* (7), 553−560.
(22) Toby, B. H. *J. Appl. Crystallogr.* **2001**, *34* (2), 210−213.3.
(23) Perdew, J. P.; Chevary, J. A.; Vosko, S. H.; Jackson, K. A.; Pederson, M. R.; Singh, D. J.; Fiolhais, C. *Phys. Rev. B* **1992**, *46*, 6671−6687.
(24) Howard, C. J.; Stokes, H. T. *Acta Crystallogr. B* **1998**, *54* (6), 782−789.
(25) Woodward, P. M. *Acta Crystallogr. B* **1997**, *53* (1), 32−43.
(26) Stokes, H. T.; Kisi, E. H.; Hatch, D. M.; Howard, C. J. *Acta Crystallogr. B* **2002**, *58* (6), 934−938.
(27) Pauling, L. *J. Am. Chem. Soc.* **1929**, *51* (4), 1010−1026.
(28) Barnes, P. W.; Lufaso, M. W.; Woodward, P. M. *Acta Crystallogr. B* **2006**, *62* (3), 384−396.
(29) Zhurova, E. A.; Ivanov, Y.; Zavodnik, V.; Tsirelson, V. *Acta Crystallogr. B* **2000**, *56* (4), 594−600.
(30) Brese, N. E.; O'Keeffe, M.; Rauch, P.; DiSalvo, F. J. *Acta Crystallogr. C* **1991**, *47*, 2291−94.
(31) Shannon, R. D.; Prewitt, C. T. *Acta. Crystallogr. B* **1969**, *25*, 925.
(32) Hyde, B. G.; O'Keeffe, M. *Acta Crystallogr. B* **1977**, *33*, 3802−13.
(33) Lufaso, M. W.; Woodward, P. M. *Acta Crystallogr. B* **2001**, *57* (6), 725−738.
(34) Ahtee, A.; Ahtee, M.; Glazer, A. M.; Hewat, A. W. *Acta Crystallogr. B* **1982**, *24*, 1968−2038.
(35) Stoltzfus, M. Ohio State University, Ph.D. dissertation, 2007.
(36) Udovenko, A. A.; Vasiliev, A. D.; Laptash, N. M. *Acta Crystallogr. B* **2010**, *66*, 34−39.
(37) Donakowski, M. D.; Gorne, A.; Vaughey, J. T.; Poeppelmeier, K. R. *J. Am. Chem. Soc.* **2013**, *135* (26), 9898−9906.
(38) Fry, A. M.; Seibel, H. A.; Lokuhewa, I. N.; Woodward, P. M. *J. Am. Chem. Soc.* **2012**, *134* (5), 2621−2625.

(39) Wheeler, R. A.; Whangbo, M. H.; Hughbanks, T.; Hoffmann, R.; Burdett, J. K.; Albright, T. A. *J. Am. Chem. Soc.* **1986**, *108* (9), 2222−2236.
(40) Sham, L. J.; Schluter, M. *Phys. Rev. B* **1985**, *32*, 3883−3889.
(41) Sun, J.; Buhro, W. E.; Wang, L.-W.; Schrier. *J. Nano Lett.* **2008**, *8*, 2913−2919.
(42) Seidl, A.; Gorling, A.; Vogl, P.; Majewski, J. A.; Levy, M. *Phys. Rev. B* **1996**, *53*, 3764−3774.
(43) Burdett, J. *Chemical Bonding in Solids, Topics in Inorganic Chemistry Series*; Oxford University Press: New York, 1995.
(44) Hoffmann, R. *Solids and Surfaces: A Chemist's View of Bonding in Extended Structures* ; VCH Publishers: New York, 1988.
(45) Dronskowski, R.; Hoffmann, R. *Computational Chemistry of Solid State Materials: A Guide for Materials Scientists, Chemists, Physicists and Others*; John Wiley & Sons: New York, 2008
(46) Shapiro, I. P. *Opt. Spektrosk.* **1958**, *4*, 256−260.
(47) Eng, H.; Barnes, P.; Auer, B.; Woodward, P. M. *J. Solid State Chem.* **2003**, *175*, 94−109.
(48) Porter, S. H.; Balaz, S.; Brillson, L.; Woodward, P. M. *Chem. Mater.* **2013**, *25*, 3337−3343.
(49) Dolgos, M. R; Paraskos, A. M.; Stoltzfus, M. W.; Yarnell, S. C; Woodward, P. M *J. Solid State Chem.* **2009**, *182*, 1964−71.

dx.doi.org/10.1021/cg401230a | *Cryst. Growth Des.* 2014, 14, 117−125